Cross Correlate Tidal Reconstructed 21cm Signal with Kinematic Sunyaev-Zel'dovich Effect: A New Probe for Missing Baryons at $z \sim 1-2$

We propose a new way to study baryon abundance and distribution at mid redshift. We cross correlate density field from HI 21cm intensity mapping with temperature anisotropy of Cosmic Microwave Background(CMB) caused by raidal motion of free electrons, i.e. kinetic Sunyaev-Zel'dovich(kSZ) effect. We put forward a 3D cosmic tidal reconstruction to recover the modes lost in 21cm foregrounds, which will effectively promote the apprearance of correlation signals.

We verify the idea with simulation outputs on $z = 1, z = 2$, taking into account of foreground substractions, facility resolutions, and redshift distortions. We successfully recover $> 90\%$ information of the 21cm density field at $k \sim 0.01h/Mpc$ after tidal reconstruction. We obtain a $r > 0.6$ correlation with origin kSZ signal from $l \sim 100 - 2000$. Assuming the noise level of Planck, the S/N will exceed 3 from $l \sim 500 - 3000$.

This is a very promissing probe to study diffused matter distribution. 1. It is less biased towards local density contraction, thanks to the kinetic nature of kSZ signals; 2. It has precise redshift information from 21cm spectrum; 3. It is rather feasible to get required data of higher redshifts with large sky coverage. The 21cm intensity mapping survey has huge advantage on survey speed, facility requirements and costs comparing to spectrocscopic galaxy survey.

Consider the simulated S/N level, data requirements, current and upcoming 21cm intensity mapping facilities, we are optimistic about the new probe.

PACS numbers:

I. INTRODUCTION

While the baryon abundance of early universe is well fixed by the cosmic microwave background (CMB),Big Bang Nucleosynthesis and Lyman-α forest [1][2][3][4], a deficiency was noiticed in local universe. At $z \lesssim 2$ the detected baryon content in collapsed objects, eg. galaxies, galaxy clusters and groups, only account for 10% of the predicted amount. More baryons are believe to reside in Warm-Hot Intergalactic Mediums (WHIM) with typical temperature of 10^5 K to 10^7 K [5][6], which is too cold and diffuse to be easily detected. Continuous effort has been made to detect this part of the baryons. One common approach is using hydrogen and metal absorption lines(eg, HI, Mg II,Si II, C II, Si III, C III, Si IV, O VI, O VII) [7][8]. However, the lines are usually limited to close circumgalactic medium, while at least 25% of the baryons are bebieved to reside in more diffused region [9]. Moreover, the uncertainty in metalicity would sometimes reduce the reliability.

A promising tool to probe the missing baryon is the kinetic Sunyaev-Zel'dovich(kSZ) effect [10][11], an effect that is greatly known for its potential to explore the Epoch of Reionization [12][13][14]. It refers to the secondary temperature anisotropy in CMB caused by radial motions of free electrons, which only correlates to electron density and velocity, regardless the temperature and pressure. Since the velocity field mainly results from large scale structure, the method is less biased towards hot, compact place, and provide more information on the fraction of diffused baryons.

Attractive as it is, due to the contamination from primary CMB and residual thermal SZ signal it is difficult to filter the kSZ signal without other sources. Worse still, the signal itself does not contain redshift information.

To fix this, previous approches cross correlated it with galaxy surveys, eg. using pairwise-momentum estimator [15] or velocity-field-reconstruction estimator [16][17]. However since they all require spectroscopy of galaxies to provide accurate redshift, the sky volume and redshift range to apply the method is limited. A recent effort try to fix this by using photometries of infrared-selected galaxies. However, since they used projected fields of the galaxies, they could only obtain a rough estimate over a wide redshift bin [18].

In this paper we present a new cross relating source, HI density field, from 21cm intensity mapping, a kind of surveys that provide integrated signals of diffuse 21cm spectra, rather than detecting individual objects.

It will make it feasible to probe the baryon content to $z \gtrsim 1$ in very near future, with ongoing experiments like CHIME [19], Tianlai [20], HIRAX [21] etc. . Besides, the 21cm spectrum contains accurate redshift information, which makes it a good candidate to be cross correlated to kSZ signals.

This powerful probe was rarely harnessed in this topic previously, because the continuum foregrounds in 21cm measurements is typically 10^2-10^3 times brighter than cosmological signals, almost completely bury the distribution of large scale structures in radial direction, i.e. modes with small $k_\parallel$. Meanwhile the veocity field is closely related with the large scale structure, which makes the correlation difficult to see.

To compensate that, a new method called *cosmic tidal reconstruction* has been developed recently [22][23]. It can reconstruct the large scale density field from the alignment of small scale cosmic structures. In this paper, we further extend the previous 2D tidal reconstruction to 3D–this is a necessity since we need more accurate large scale density field on z directions. We discuss the influence of redshift distortions for that.

Applying this methods to foreground substracted 21cm density fields, we obtain a sufficiently good cross-correlation signal with original kSZ signals.

The paper is organized as follows: In section II, we introduce general algorithm, including 3D tidal reconstruction, velocity reconstruction and cross correlation with kSZ signal; In section III, we address the simulation results at redshift 1 and 2; In section IV, we discuss statistical errors and redshift

distortions; In section V, we give conclusions.

II. RECONSTRUCTION ALGORITHM

A. 3D Cosmic Tidal Reconstruction

While a cosmic signal in 21cm measurement is of the order of mK, foregrounds coming from Galactic emissions, telescope noise, extragalactic radio sources and Radio recombination lines, can reach the order of Kelvin [24][25]. Lots of techniques have been developed to substract the foregrounds, taking advantage of the attribute that they have fewer bright spectral degrees of freedom[26]. Unfortunately, the substraction usually contaminates the smooth large scale structure information. Since the large scale information is essential for the estimate of peculiar velocity, we need to recover the information. However, since large scale structure is correlated closely to the emergence of peculiar velocity, we need a method to estimate its distribution.

The cosmic tidal reconstruction is a kind of quadratic statistics developed to achieve this goal. Its main idea is using small scale filamentary structures to solve for the large scale tidal shear and gravitational potential.

Here, we present a 3 dimentional reconstruction algorithm that works best in close linear regions.

First, we filter for the small scale structures that are most likely to be influenced by tidal force of large scale fields.

(1) Convolve the field with a Gaussian kernal $S(\boldsymbol{k}) = e^{-k^2R^2/2}$, we take $R = 1.25\ \mathrm{Mpc}/h$ [22], to reduce the complicated non-linear effects on small scales.

(2) Gaussianize the field, taking $\delta_g = \ln(1+\delta)$. This is to allieviate the problem that filter W_i in (3) heavily weights high density regions.

(3) Apply filter $W_i(\boldsymbol{k})$, which assigns weights to δ_g according to predicted displacements caused by tidal field in near linear regions [23]. $\delta_g^{w_i}(\boldsymbol{k}) = W_i(\boldsymbol{k})\delta_g(\boldsymbol{k})$,

$$W_i(\boldsymbol{k}) = i(\frac{P(k)f(k)}{P_{tot}^2(k)})^{\frac{1}{2}}\frac{k_i}{k} = S(k)\frac{k_i}{k} \tag{1}$$

i indicates $\hat{x}, \hat{y}, \hat{z}$ directions, $P_{tot} = P + P_{noise}$ is observed matter powerspectrum, P is theoretical matter powerspectrum, $f = 2\alpha(\tau) - \beta(\tau) dlnP/dlnk$, where α and β are functions related to linear growth funcion, and are calculated to be (0.6, 1.3) for $z = 1$ and (0.4, 0.9) for $z = 2$. [1]

Second, we estimate the tidal force and hense reconstruct the large scale density field.

(1) Following gravitational lensing procedures, we decompose the 3×3 symmetric, traceless tidal force tensor into 5 γ components, and estimate them from density variance.

$$\begin{aligned}
\hat{\gamma}_1(\boldsymbol{x}) &= [\delta_g^{w_1}(\boldsymbol{x})\delta_g^{w_1}(\boldsymbol{x}) - \delta_g^{w_2}(\boldsymbol{x})\delta_g^{w_2}(\boldsymbol{x})], \\
\hat{\gamma}_2(\boldsymbol{x}) &= [2\delta_g^{w_1}(\boldsymbol{x})\delta_g^{w_2}(\boldsymbol{x})], \\
\hat{\gamma}_x(\boldsymbol{x}) &= [2\delta_g^{w_1}(\boldsymbol{x})\delta_g^{w_3}(\boldsymbol{x})], \\
\hat{\gamma}_y(\boldsymbol{x}) &= [2\delta_g^{w_2}(\boldsymbol{x})\delta_g^{w_3}(\boldsymbol{x})], \\
\hat{\gamma}_z(\boldsymbol{x}) &= [(2\delta_g^{w_3}(\boldsymbol{x})\delta_g^{w_3}(\boldsymbol{x}) - \delta_g^{w_1}(\boldsymbol{x})\delta_g^{w_1}(\boldsymbol{x}) - \delta_g^{w_2}(\boldsymbol{x})\delta_g^{w_2}(\boldsymbol{x}))]/3,
\end{aligned} \tag{2}$$

(2) Reconstruct 3D density field.

$$\begin{aligned}
\kappa_{3\mathrm{D}}(\boldsymbol{k}) &= \frac{1}{k_1^2+k_2^2+k_3^2}[(k_1^2-k_2^2)\gamma_1(\boldsymbol{k}) + 2k_1k_2\gamma_2(\boldsymbol{k}) \\
&\quad +2k_1k_3\gamma_x(\boldsymbol{k}) + 2k_2k_3\gamma_y(\boldsymbol{k}) + (2k_3^2-k_1^2-k_1^2)\gamma_z(\boldsymbol{k})].
\end{aligned} \tag{3}$$

Third, we correct bias and suppress noise with a Wiener filter. Due to the foregrounds, the noise in z direction will be different from x,y direction, therefore we apply an anisotropic Wiener filter.

$$\hat{\kappa}_c(\boldsymbol{k}) = \frac{\kappa_{3D}(\boldsymbol{k})}{b(k_\perp, k_\parallel)}W(k_\perp, k_\parallel)\ , \tag{4}$$

Bias $b = \frac{P_{k3D\delta}}{P_\delta}$, Wiener filter $W = \frac{P_\delta}{P_{k3D}/b^2}$.

Here and afterwards, we use "$\wedge$" to denote recontructed fields.

B. Velocity Reconstruction and kSZ signals

Due to the cancellation of positive and negative velocity, direct cross correlation between kSZ signal and density field is hard to see. Therefore, we first estimate the peculiar velocity from the 3D density field, then construct the 2D map of kSZ signal, and correlate it with the real kSZ signal [16].

Detailed steps are as follows.

(1) Estimate the velocity field:

In linear region, the continuity equation goes like: $\dot{\delta} + \nabla \cdot \boldsymbol{v} = 0$, where $\boldsymbol{v}$ is the peculiar velocity and δ is the matter overdensity.

Therefore, we obtain an estimator of velocity distribution:

$$\hat{v}_z(\boldsymbol{k}) = iaHf\delta(\boldsymbol{k})\frac{k_z}{k^2} \tag{5}$$

where $f = \frac{d\ln D}{d\ln a}$, D(a) is the linear growth function, a is the scale factor, H is the Hubble parameter.

$v_z \propto \frac{k_z}{k^2}$, indicating the most prominent signal comes from small k mode, which corresponds to large scale structure. This further verify our motivation for tidal reconstruction procedure.

(2) suppress the noise in velocity field with a new Wiener filter, following identical procedure as Eq.(4). This is because the term $\frac{k_z}{k^2}$ in Eq.(5) will strongly amplify noises in small k modes.

(3) Calculate 2D kSZ map.

The CMB temperature fluctuations caused by kSZ effect is:

$$\Theta_{kSZ}(\hat{n}) \equiv \frac{\Delta T_{kSZ}}{T_{\mathrm{CMB}}} = -\frac{1}{c}\int d\eta g(\eta)\boldsymbol{p}_\parallel\ , \tag{6}$$

[1] The effect of the filter W_i on different scales could be seen in Appendix 1.

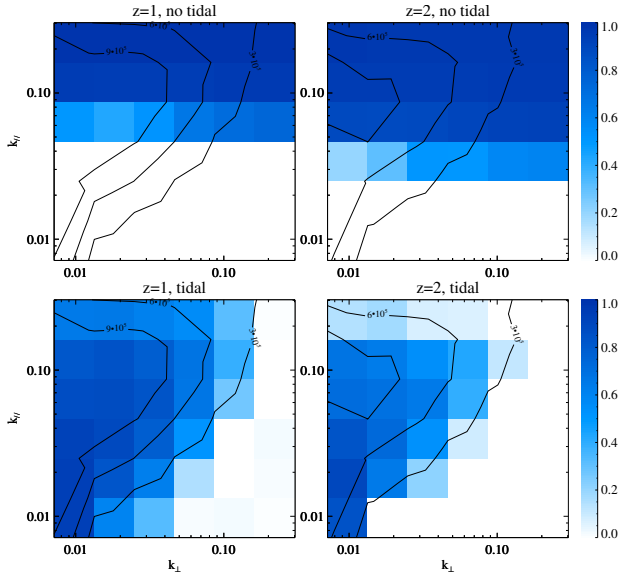

FIG. 1: (Top) The cross correlation r between P_{v_z} and $P_{\hat{v}_z^{fs}}$ calculated from foreground substracted field δ_{fs}; (Bottom) The cross correlation between P_{v_z} and $P_{\hat{v}_z^{tide}}$ calculated from $\hat{\kappa}_c$. The contour line indicates $k^3P(k)$.

where $\eta(z)$ is the comoving distance at redshift z, $g(\eta) = e^{-\tau}d\tau/d\eta$ is the visibility function, τ is the optical depth to Thomson scattering, $\boldsymbol{p}_\parallel = (1+\delta)\boldsymbol{v}_\parallel$, with δ the electron overdensity. We assume that $g(\eta)$ doesn't change significally in one redshift bin, and integrate $\boldsymbol{p}_\parallel$ along radial axis to get $\hat{\Theta}_{kSZ}$

(4) Calculate correlation coefficients.

We compare reconstructed kSZ signals $\hat{\Theta}_{kSZ}$ with kSZ signals Θ_{kSZ} directly from simulations. To quantify the tightness of correlation, we employ a quantity r:

$$r \equiv \frac{P_{recon,real}}{\sqrt{P_{recon}P_{real}}} \tag{7}$$

III. SIMULATIONS

A. Simulation Set up

We use six N-body simulations from the CUBEP^{3}M code [27], each evolving 1024^3 particles in a $(1.2\mathrm{Gpc}/h)^3$ box. We assume Hubble parameter $h = 0.678$, baryon density $\Omega_b = 0.049$, dark matter density $\Omega_c = 0.259$, amplitude of primordial curvature power spectrum $A_s = 2.139 \times 10^{-9}$ at $k_0 = 0.05$ Mpc^{-1} and scalar spectral index $n_s = 0.968$. We analyse the outputs at redshift 1 and 2.

To ressemble realistic observations:

1. We import a cut off scale k_c, assume that modes with $k > k_c$ are not resolved. This is reasonable for a filled aperture experiment, which has good brightness sensitivity and an exponetially growing noise at small scales. We choose $k_c = 0.5\ h/\mathrm{Mpc}$ and $0.32h/\mathrm{Mpc}$ respectively for $z = 1$ and $z = 2$, which corresponds to $\ell \sim 1150$. This is generally realistic, judging from ongoing 21cm experiments like CHIME [19][28] and Tianlai [29][20].

2. We use a high pass filter $W_{fs}(k_\parallel) = 1 - e^{-k_\parallel^2 R_\parallel^2/2}$ to imitate the foreground substraction. We choose $R_\parallel = 15\,\mathrm{Mpc}/h$ for $z = 1$ and $R_\parallel = 8\ \mathrm{Mpc}/h$ for $z = 2$, which gives $W_{fs} = 0.5$ at $k_\parallel = 0.08\ \mathrm{Mpc}/h$ and $0.15\ \mathrm{Mpc}/h$ respectively.

The observed 21cm field after foreground subtraction is then given by

$$\delta_{fs}(\boldsymbol{k}) = \delta(\boldsymbol{k})W_{fs}(k_\parallel)J(k_c - k), \tag{8}$$

where $\delta(\boldsymbol{k})$ is the original density field, $J(x)$ equals 0 for $x < 0$ and equals 1 elsewhere.

After that, we reconstruct the large scale fields $\hat{\kappa}_c$ from δ_{fs} via cosmic tidal reconstruction. We use $\hat{\kappa}_c$ to obtain an estimate radial velocity field $\hat{v}_z^{tide}$ follow Eq.(5). We reconstruct the kSZ signal $\hat{\Theta}^{tide}$ following Eq.(6) and compare it with kSZ signal.

To show the effects of tidal reconstruction, we go through the same procedure for δ_{fs} and get $\hat{\Theta}fs$.

B. Results

1. Correlation of reconstructed velocity fields:

We first present the result about reconstructed velocity field(Eq.(5)) in Fig.1. The upper two panels show the cross correlation r between v_z and $\hat{v}_z^{fs}$ calculated from foreground substracted field δ_{fs}; the lower panel shows the cross correlation between v_z and $\hat{v}_z^{tide}$ calculated from $\hat{\kappa}_c$. The contour line represent the value of $k^3P(k)$, which is related to the importance of each mode when generating kSZ signals.

Notice: 1. Although the foreground at z=2 is stronger, the non-linear effects are weaker. Therefore, we can still see some correlations at $k\ \|\lesssim 0.1$, with the little density signals left. And these correlations are even better than the z=1 case after the gaussianization.

On the other hand, there is degrading performance of tidal reconstruction on z=2. This is likely due to the stricter cutoff $k_c = 0.32h/Mpc$ compared to $k_c = 0.5h/Mpc$ at z=1.

2. Since tidal reconstruction relies strongly on large k modes, and we only lost small k_z modes in the foreground(Fig.1 upper panel). The reconstruction on $k_\parallel$ is better than on $k_\perp$, which is an advantage for estimating v_z.

Important to see: 1. The previously lost small $k_\parallel$ modes has been well reconstructed through the 3D tidal reconstruction procedures. 2. The modes recovered in tidal reconstruction play more vital role in generating kSZ signals.

2. Correlation of reconstructed kSZ signals:

In Fig.2, we demonstrate the correlation r between the reconstructed kSZ signal $\hat{\Theta}$ and original kSZ signal Θ (black lines). We used both orginal foreground substracted density field and tidal reconstructed density field and compare the different results.

Important to see: 1. For z=1, there are significant improvement on the cross-correlation after tidal reconstruction, especially below $l \sim 2000$ 2. For z=2, the tidal reconstruction

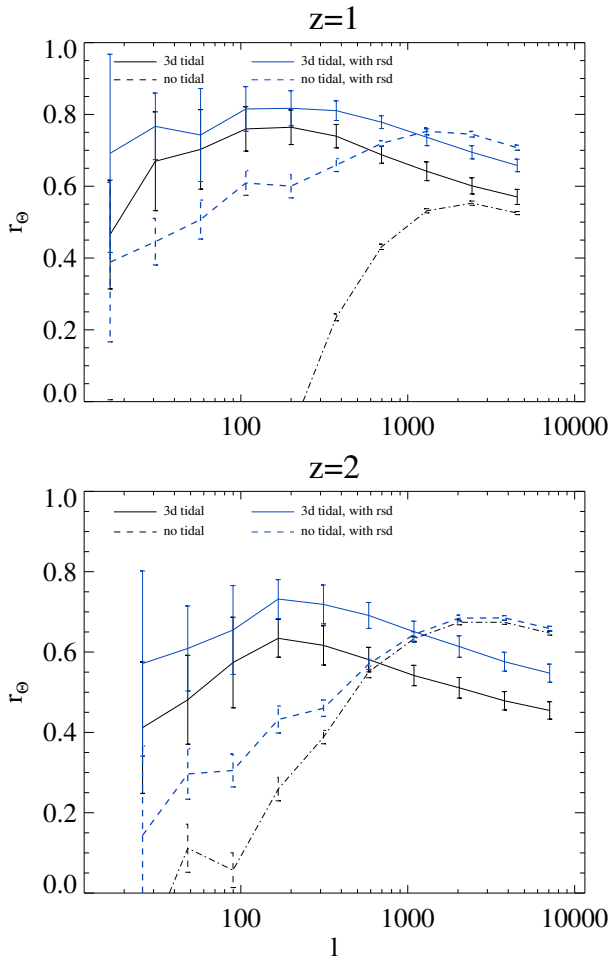

FIG. 2: The cross correlation r between reconstructed kSZ $P_{\hat{\Theta}_{kSZ}}$ and real kSZ $P_{\Theta_{kSZ}}$. (Dashed line) kSZ calculated from foreground substracted 21cm density field δ_{fs}; (Solid line) kSZ calculated from tidal reconstructed density field. (Blue lines) take into account of redshift distortions.

improves the cross-correlation for $l \lesssim 800$. However, since the non-linear effect is less strong at this stage, the orginal 21cm density field is good enough to reconstruct kSZ signal for $l \gtrsim 800$. Combining them, we would have good cross-correlation for $l \sim 20 - 8000$.

In all, for both redshift, with the non-ideal foregrounds and resolutions we assume, we are able to obtain a correlation $r \gtrsim 0.5$ for $l \sim 50 - 5000$ between 21cm density field and kSZ signals.

IV. DISCUSSION AND ERROR ESTIMATES

A. Redshift Distortion

We analyze the influence of linear redshift space distortion (RSD) in kSZ signal reconstruction. Equipped with it, we provide the very interesting results of adding RSD to simulations, and get better cross correlation (Fig.2). We also discuss another important advantage RSD brings.

The redshift distortions results from the radial peculiar velocity, which leads to a misjudgement of distance referring to Hubble flow.

In linear regions, it will induce an extra density contraction in redshift space:

$$\delta^{RSD}(\boldsymbol{k}) \approx (1 + f\frac{k_z^2}{k^2})\delta(\boldsymbol{k}) \tag{9}$$

where again $f = \frac{d\ln D}{d\ln a}$, with the cosmological parameter we choose, $f = 1.5, z \sim 1; f = 0.96, z \sim 2$.

Therefore, the easiest way to substract the linear RSD is to devide the δ^{RSD} we have by $1 + f\frac{k_z^2}{k^2}$ before all the calculations.

However, if we leave it here, since our foreground is in the same direction as the RSD, we will see some fortunate good effects. We discuss both the case of non-tidal reconstruction, and tidal reconstruction, and they are improved in different ways.

Note: in the following argument, small k refers to $k \sim 0.01h/Mpc$, larger k refers to $k > 0.1h/Mpc$, the powerspectrum of latter is around a magnitude smaller than the former.

(1) $\hat{\Theta}$ with RSD foreground substracted 21cm density field δ_{fs}^{RSD}.

Following Eq.(5), we can quickly write down the change for v(k):

$$\hat{v}_{z,fs}^{RSD}(\boldsymbol{k}) \propto \delta_{fs}^{RSD}(\boldsymbol{k})\frac{k_z}{k^2} \tag{10}$$

$$= \hat{v}_{z,fs}(\boldsymbol{k})(1 + f\frac{k_z^2}{k^2}) \tag{11}$$

The new term gives heavier weigh to modes with $k_\parallel \gg k_\perp$.

The real kSZ signal in Fourier space reads:

$$\Theta(\boldsymbol{k}_\perp) \equiv \Theta(k_x, k_y, 0) \propto \int d^3k \quad \delta(\boldsymbol{k}_\perp - \boldsymbol{k})v_z(\boldsymbol{k}) \tag{12}$$

$$\propto \int d^3k \;\; \delta(\boldsymbol{k}_\perp - \boldsymbol{k})\delta(\boldsymbol{k})\tfrac{k_z}{k^2}$$

For foreground substracted field the kSZ signal in Fourier space becomes:

$$\Theta_{fs}^{RSD}(\boldsymbol{k}_\perp) \propto \int d^3k \;\; \delta(\boldsymbol{k}_\perp - \boldsymbol{k})\delta_{fs}(\boldsymbol{k})\tfrac{k_z}{k^2}(1 + f\tfrac{k_z^2}{k^2}) \tag{13}$$

Notice, the first δ we use the original field, since this is the quantity we want to obtain in real cross correlating procedures.

seems to need a powerspectrum of P_δ

When $k_\perp$ is small:

In original kSZ signal, $\delta(\boldsymbol{k}_\perp - \boldsymbol{k}), \delta(\boldsymbol{k}), \frac{k_z}{k^2}$ reaches peak nearly at the same point when both $k_\perp, k \;\|$ are small, and this dominates the signal. However, in the case of foreground substracted field, δ_{fs} is seriously reduced at small $k_\parallel$, and Θ_{fs} hense comes more from larger $k_\parallel$ which has little correlations with the original kSZ.

Fortunately, the RSD gives another term $1 + f\frac{k_z^2}{k^2}$, which give additional weigh to smaller $k_\parallel$ and partly compensate the

weigh loss in foreground substraction. Therefore, we could have slightly better correlations in small $k_\perp$.

When $k_\perp$ is large:

$\delta(\boldsymbol{k}_\perp - \boldsymbol{k})$ and $\delta(\boldsymbol{k})$ no longer reach the peak simultaneously, and Θ comes from sum of a series of $k\prime$ from small to larger, hense the foreground substraction does not matter as much as in the case of $k_\parallel$, so both RSD and non-RSD case will have cross correlation.

(2) RSD influence to tidal reconstruction

After adding linear RSD, Eq.(2), each term will have two new weigh in Fourier space.

For simplicity, we define a demonstrator $\hat{\gamma}^{RSD}_{i,j}(\boldsymbol{x}) \equiv \delta^{w_i}_{RSD}(\boldsymbol{x})\delta^{w_j}_{RSD}(\boldsymbol{x})$.

In Fourier space, it becomes:

$$\hat{\gamma}_{RSD}(\boldsymbol{k}) = \int \frac{d^3k\prime}{(2\pi)^3}\delta^{w_i}(\boldsymbol{k}-\boldsymbol{k\prime})\delta^{w_j}(\boldsymbol{k\prime}) \tag{14a}$$
$$(1+f\frac{(\boldsymbol{k}-\boldsymbol{k\prime})^2_z}{(\boldsymbol{k}-\boldsymbol{k\prime})^2})(1+f\frac{k\prime^2_z}{k\prime^2})$$
$$= \int \frac{d^3k\prime}{(2\pi)^3}\delta_{fs}(\boldsymbol{k}-\boldsymbol{k\prime})S(|\boldsymbol{k}-\boldsymbol{k\prime}|)\delta_{fs}(\boldsymbol{k\prime})S(k\prime) \tag{14b}$$
$$\frac{(\boldsymbol{k}-\boldsymbol{k\prime})_i}{|\boldsymbol{k}-\boldsymbol{k\prime}|}\frac{k\prime_j}{k\prime}(1+f\frac{(\boldsymbol{k}-\boldsymbol{k\prime})^2_z}{(\boldsymbol{k}-\boldsymbol{k\prime})^2})(1+f\frac{k\prime^2_z}{k\prime^2})$$

From (14a) we can see that the shear estimators now favor information from $\delta(k)$ with $k\_parallel \gg k_\perp$ more than before.

From (14b) we see the influence on different gamma varies. The amplification will be maximized when the shape of the two new weigh $(1+f\frac{k_z}{k^2}$ at most approches other terms, i.e. when $i=j=z$. Therefore $\hat{\gamma}_z$ will be influenced most, followed by $\hat{\gamma}_x, \hat{\gamma}_y$

In all, the RSD effect is a natual filter that weighs more the information on z direction, and down-weigh the information of large $k_\perp$ to small $k_\perp$.

Therefore, if we use 2D tidal reconstruction, RSD will cause a noticeable degration on the reconstruction (If we have RSD yet not have foreground, apply 3D tidal reconstruction, RSD may cause slight degration with However, fortunately, we have foreground which happen to be in the same direction with RSD. For z directions, only small $k_\parallel$ modes are lost, which do not matter much in the reconstruction; while for other directions sufficient amount of modes with $k_\perp$ from small to large are lost, and this leads to more inaccurate reconstruction on $k_\perp$ direction. And RSD serve as a natural filter to deal with that. 1

B. Statistical Error

We use the statistical error to estimate the S/N ratio for real surveys. Taking into account the contamination from primary CMB and facility noises, it can be approximated as:

$$\frac{\Delta C_l}{C_l} \simeq \frac{1}{r\sqrt{(2l+1)\Delta l f_{sky}}}\sqrt{\frac{C_l^{\rm CMB}+C_l^{kSZ}+C_l^{\rm CMB,N}}{C_l^{kSZ,\Delta z}}} \tag{15}$$

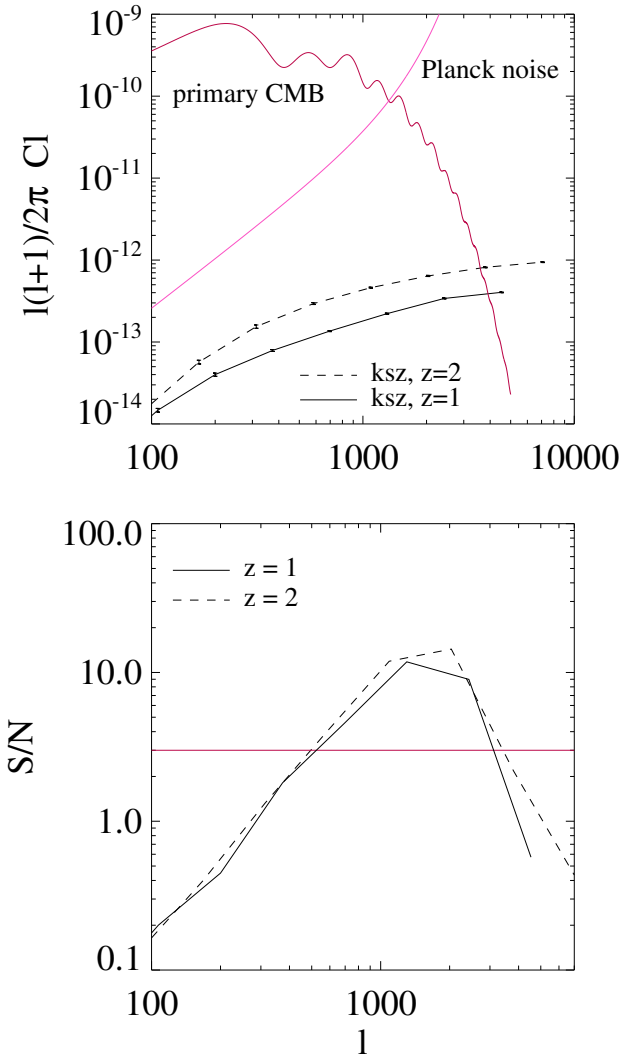

FIG. 3: (Top) Relative strength of kSZ signal, within a box of $\Delta\chi = 1200Mpc/h$. (Bottom) predicted S/N, assuming Planck noise, $\Delta l/l = 0.1$, $f_{sky} = 0.8$.

Where C_l^{CMB} is the angular powerspectrum of primary CMB; $C_l^{CMB,N}$ indicates the facility noises; $C_l^{kSZ,\Delta z}$ is the kSZ signal from a certain redshift bin; r is the correlation coefficients we get; f_{sky} is the percent of sky area covered by both surveys.

In our case, we calculate C_l^{CMB} from CAMB [30]. We use Planck 2015 results [31] at 217GHz to estimate $C_l^{CMB,N}$. $C_l^{CMB,N} = (\sigma_{p,T}\theta_{FWHM})^2 W_l^{-2}$; where $\sigma_{p,T} = 8.7\mu K_{CMB}$ is Sensitivity per beam solid angle, $\theta_{FWHM} \sim 5'$ is the effective beam FWHM, $W_l = exp[-l(l+1)/2l^2_{beam}]$ is the smoothing window function, with $l_{beam} = \sqrt{8\ln 2}/\theta_{FWHM}$. We choose $f_{sky} = 0.8$, since it is feasible for 21cm intensity mapping to survey large sky areas. We choose $\Delta l/l = 0.1$. And for $C_l^{kSZ,\Delta z}$, we choose two bins of size 1200 Mpc/h, centered at redshift 1,2 respectively.

In Fig.3, we plot the S/N level for the two redshift bins. The

S/N will exceeds 3 from $l \sim 500 - 3000$.

Since we only use the correlation calculated from tidal reconstructed field, the S/N shall be higher for z=2 combining tidal reconstructed field and foreground substracted field. Moreover, since C_l^{kSZ} is relatively flat, it is possible to bin it into larger Δl. eg. [18] choose $\Delta l = 200$, and this will yield better S/N for $l < 2000$ in Fig.3.

What's more, Planck's noise level is far from ideal. If we consider the case of 4th generation facilities, there will also be a giant leap for S/N at large l. However, in that case, we have to have accurate substraction for CMB lensing, when primary CMB dims out.

V. CONCLUSION

VI. ACKNOWLEDGE

We acknowledge discussions with Kendrick Smith, Matthew Johnson, Wenkai Hu, Tianxiang Mao and Jiawei Shao. The simulations were performed on the BGQ supercomputer at the SciNet HPC Consortium. SciNet is funded by: the Canada Foundation for Innovation under the auspices of Compute Canada; the Government of Ontario; the Ontario Research Fund – Research Excellence; and the University of Toronto. Research at the Perimeter Institute is supported by the Government of Canada through Industry Canada and by the Province of Ontario through the Ministry of Research Innovation. The Dunlap Institute is funded through an endowment established by the David Dunlap family and the University of Toronto.

[1] R. J. Cooke, M. Pettini, R. A. Jorgenson, M. T. Murphy, and C. C. Steidel, ApJ **781**, 31 (2014), 1308.3240.
[2] G. Hinshaw, D. Larson, E. Komatsu, D. N. Spergel, C. L. Bennett, J. Dunkley, M. R. Nolta, M. Halpern, R. S. Hill, N. Odegard, et al., ApJS **208**, 19 (2013), 1212.5226.
[3] E. Komatsu, K. M. Smith, J. Dunkley, C. L. Bennett, B. Gold, G. Hinshaw, N. Jarosik, D. Larson, M. R. Nolta, L. Page, et al., ApJS **192**, 18 (2011), 1001.4538.
[4] G. Hinshaw, D. Larson, E. Komatsu, D. N. Spergel, C. L. Bennett, J. Dunkley, M. R. Nolta, M. Halpern, R. S. Hill, N. Odegard, et al., ApJS **208**, 19 (2013), 1212.5226.
[5] U.-L. Pen, ApJ **510**, L1 (1999), astro-ph/9811045.
[6] A. M. Sołtan, A&A **460**, 59 (2006), astro-ph/0604465.
[7] M. Fukugita and P. J. E. Peebles, ApJ **616**, 643 (2004), astro-ph/0406095.
[8] J. K. Werk, J. X. Prochaska, J. Tumlinson, M. S. Peeples, T. M. Tripp, A. J. Fox, N. Lehner, C. Thom, J. M. O'Meara, A. B. Ford, et al., ApJ **792**, 8 (2014), 1403.0947.
[9] R. Davé, B. D. Oppenheimer, N. Katz, J. A. Kollmeier, and D. H. Weinberg, MNRAS **408**, 2051 (2010), 1005.2421.
[10] R. A. Sunyaev and Y. B. Zeldovich, Comments on Astrophysics and Space Physics **4**, 173 (1972).
[11] R. A. Sunyaev and I. B. Zeldovich, MNRAS **190**, 413 (1980).
[12] P. Zhang, U.-L. Pen, and H. Trac, MNRAS **347**, 1224 (2004), astro-ph/0304534.
[13] M. McQuinn, S. R. Furlanetto, L. Hernquist, O. Zahn, and M. Zaldarriaga, ApJ **630**, 643 (2005), astro-ph/0504189.
[14] O. Zahn, C. L. Reichardt, L. Shaw, A. Lidz, K. A. Aird, B. A. Benson, L. E. Bleem, J. E. Carlstrom, C. L. Chang, H. M. Cho, et al., ApJ **756**, 65 (2012), 1111.6386.
[15] N. Hand, G. E. Addison, E. Aubourg, N. Battaglia, E. S. Battistelli, D. Bizyaev, J. R. Bond, H. Brewington, J. Brinkmann, B. R. Brown, et al., Physical Review Letters **109**, 041101 (2012), 1203.4219.
[16] J. Shao, P. Zhang, W. Lin, Y. Jing, and J. Pan, MNRAS **413**, 628 (2011), 1004.1301.
[17] M. Li, R. E. Angulo, S. D. M. White, and J. Jasche, MNRAS **443**, 2311 (2014), 1404.0007.
[18] J. C. Hill, S. Ferraro, N. Battaglia, J. Liu, and D. N. Spergel, ArXiv e-prints (2016), 1603.01608.
[19] K. Bandura, G. E. Addison, M. Amiri, J. R. Bond, D. Campbell-Wilson, L. Connor, J.-F. Cliche, G. Davis, M. Deng, N. Denman, et al., in *Society of Photo-Optical Instrumentation Engineers (SPIE) Conference Series* (2014), vol. 9145 of *Society of Photo-Optical Instrumentation Engineers (SPIE) Conference Series*, p. 22, 1406.2288.
[20] Y. Xu, X. Wang, and X. Chen, ApJ **798**, 40 (2015), 1410.7794.
[21] http://www.acru.ukzn.ac.za/ hirax/.
[22] U.-L. Pen, R. Sheth, J. Harnois-Deraps, X. Chen, and Z. Li, ArXiv e-prints (2012), 1202.5804.
[23] H.-M. Zhu, U.-L. Pen, Y. Yu, X. Er, and X. Chen, ArXiv e-prints (2015), 1511.04680.
[24] T. Di Matteo, B. Ciardi, and F. Miniati, MNRAS **355**, 1053 (2004), astro-ph/0402322.
[25] K. W. Masui, E. R. Switzer, N. Banavar, K. Bandura, C. Blake, L.-M. Calin, T.-C. Chang, X. Chen, Y.-C. Li, Y.-W. Liao, et al., ApJ **763**, L20 (2013), 1208.0331.
[26] E. R. Switzer, T.-C. Chang, K. W. Masui, U.-L. Pen, and T. C. Voytek, ApJ **815**, 51 (2015), 1504.07527.
[27] J. Harnois-Déraps, U.-L. Pen, I. T. Iliev, H. Merz, J. D. Emberson, and V. Desjacques, MNRAS **436**, 540 (2013), 1208.5098.
[28] L. B. Newburgh, G. E. Addison, M. Amiri, K. Bandura, J. R. Bond, L. Connor, J.-F. Cliche, G. Davis, M. Deng, N. Denman, et al., in *Society of Photo-Optical Instrumentation Engineers (SPIE) Conference Series* (2014), vol. 9145 of *Society of Photo-Optical Instrumentation Engineers (SPIE) Conference Series*, p. 91454V, 1406.2267.
[29] X. Chen, International Journal of Modern Physics Conference Series **12**, 256 (2012), 1212.6278.
[30] A. Lewis, A. Challinor, and A. Lasenby, Astrophys. J. **538**, 473 (2000), astro-ph/9911177.
[31] Planck Collaboration, R. Adam, P. A. R. Ade, N. Aghanim, M. Arnaud, M. Ashdown, J. Aumont, C. Baccigalupi, A. J. Banday, R. B. Barreiro, et al., ArXiv e-prints (2015), 1502.01587.